JOURNAL OF MATERIALS SCIENCE 33 (1998) 3285–3291

Quasi-static and dynamic compression behaviour of an FP™ alumina-reinforced aluminium metal matrix composite

M. GUDEN
Izmir Yuksek Teknoloji Enstitusu, Gaziosmanpassa Bulvari No: 16, Cankaya, Izmir, TURKEY
I. W. HALL
Departments of Mechanical Engineering and Materials Science and Engineering, University of Delaware, Newark, DE 19716, USA
E-mail: hall@me.udel.edu

An aluminium metal matrix composite reinforced with continuous unidirectional α-alumina fibres has been compression tested at quasi-static and dynamic strain rates. In the transverse direction, the composite showed increasing flow stress (at 5% strain) and maximum stress within the studied strain rates, 10^{-3}–$3 \times 10^{3}\,s^{-1}$. In the longitudinal direction, the maximum stress of the composite increased similarly with increasing strain rates within the range 10^{-5}–$7 \times 10^{2}\,s^{-1}$. It is shown that, if brooming of the sample ends can be suppressed, the failure stress of the composite in longitudinal compression increases significantly. Metallographic observations reveal the typical modes of damage initiation in the composite. © *1998 Kluwer Academic Publishers*

1. Introduction

The high strain-rate mechanical response of metal matrix composites (MMCs), as well as other composites, is important for several reasons. In engineering design, the mechanical property data of materials are frequently only available for quasi-static test conditions in which the rate of loading is very small. However, impact loading or any increase in the rate of loading during service may greatly affect the mechanical property response of the material. Therefore, in order to estimate the dynamic mechanical response of materials under sudden impact conditions, dynamic properties of the materials must be considered in order to prevent unexpected failure during service. It is envisaged that, through a systematic series of high strain-rate studies on different kinds of MMCs, it will eventually be possible to develop constitutive equations to allow the modelling of mechanical properties of new MMCs and composites. Such a predictive capability would allow the design of composites with improved or tailored high strain-rate property response.

The on-going experimental programme on high strain-rate deformation behaviour of MMCs in this laboratory is aimed at establishing such a general knowledge base of their high strain-rate behaviour. Typical MMCs tested to date include short-fibre, particulate, whisker and long-fibre reinforced MMCs. The present report concerns the results of a study of MMCs containing unidirectional fibres tested at high strain rates, as well as at quasi-static strain rates. The particular composite material chosen was an FP™/Al-reinforced MMC, a class of composite for which there is an almost complete lack of prior high strain-rate test data.

2. Materials and testing methods

The FP™ (99% α-alumina)/Al composite was produced by DuPont Company using a molten metal infiltration technique. In this technique, the FP tape was prepared using a fugitive organic binder and then tapes were laid up in the desired orientation, fibre volume fraction and overall form. After burning away the binder, molten metal was infiltrated through the network of FP fibres in a steel mould [1].

The composite contained 35 vol % (V_f%) unidirectional fibres and 3% Li in the aluminium matrix. The presence of lithium provides wetting of FP fibres by aluminium. The continuous FP fibres were 20 μm diameter. The typical microstructure of the composite in the fibre plane is shown in Fig. 1.

As-received composite was in the form of 15 mm thick plate. Slices were cut normal and parallel to the fibre plane using a diamond saw and cylindrical specimens were core drilled from these slices in orientations corresponding to the longitudinal and transverse directions. Specimens tested in the transverse direction had an aspect ratio (length/diameter) of ~0.5 and a diameter of 8.2 mm. Somewhat longer and thinner specimens were tested in the longitudinal direction, 12 mm long and 6.6 mm diameter.

Quasi-static compression tests were conducted using a screw-driven Instron machine. High strain-rate

0022–2461

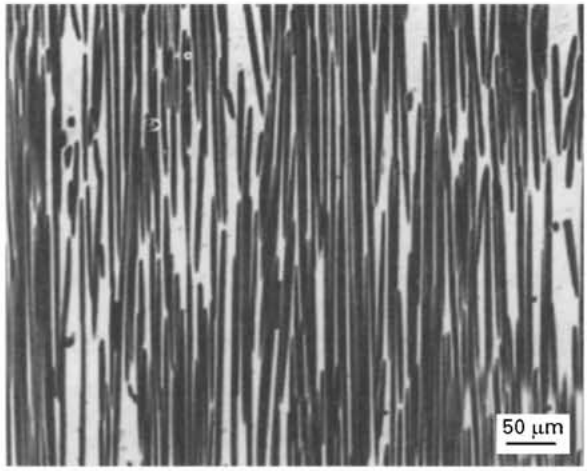

Figure 1 Optical micrograph of untested FP/Al composite in the fibre plane.

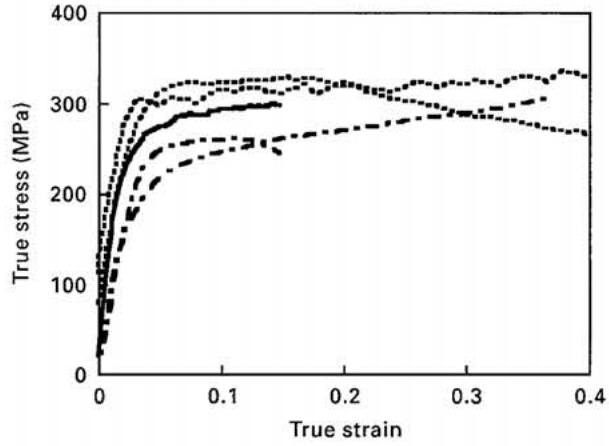

Figure 2 Typical stress–strain curves of the FP/Al composite tested in the transverse direction at different strain rates: (- - -) 2×10^3–$3 \times 10^3\,s^{-1}$; (——) $4 \times 10^2\,s^{-1}$; (–·–) $10^{-3}\,s^{-1}$.

tests were carried out in a compression type Split Hopkinson Pressure Bar (SHPB). Details of the specific SHPB used, its operation, and the procedures for data reduction are given elsewhere [2, 3]. In addition to the conventional tests, reloading tests were carried out in which samples are tested to a specific strain at one strain-rate and then retested to a higher strain at the same or another strain-rate. Such tests have several applications: for example, they are capable of showing the effects of adiabatic heating on the mechanical response of the specimen, because the sample is allowed to cool between tests. Discontinuity in the stress–strain curve between tests must, therefore, be due to effects such as heating, inertial effects, dynamic recrystallization or other microstructural response.

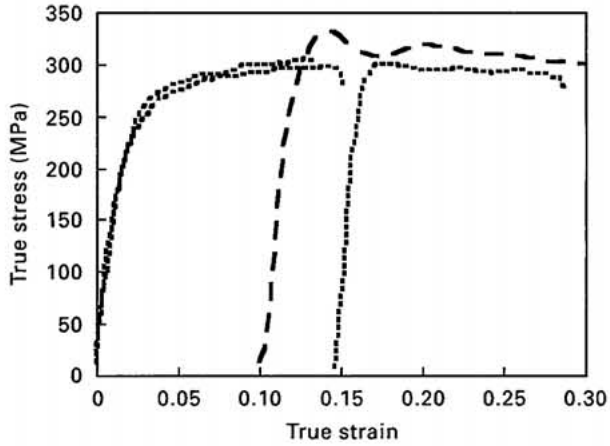

Figure 3 Typical results of reloading tests on SHPB in the transverse direction. (– – –) $3000\,s^{-1}$, (- - -) $400\,s^{-1}$.

3. Results

3.1. Transverse direction

Typical quasi-static and high strain-rate compression stress-strain curves of the composite in the transverse direction are presented in Fig. 2 which shows that the dynamic stress values are relatively high compared to the quasi-static stress values. In some of these tests, samples failed at relatively low strains after showing a peak or maximum stress as seen in Fig. 2. Early damage formation in those samples is believed to be due to local inhomogeneities such as fibre clustering and porosity at fibre–matrix interfaces resulting from incomplete infiltration and wetting.

Typical reloading tests results are shown in Fig. 3. Samples initially tested at $4 \times 10^2\,s^{-1}$ in the SHPB until about 10%–15% strain were re-strained at 4×10^2 and $3 \times 10^3\,s^{-1}$. As clearly shown in Fig. 3, at dynamic strain rates the flow stress of the composite in the transverse direction is quite rate-sensitive.

Fig. 4 shows the general results presented conventionally as flow stress values at 5% strain and the maximum stress values derived from failed samples plotted as a function of the logarithm of the strain rate. The flow stress values increased ~ 80 MPa from 10^{-3}–$3 \times 10^3\,s^{-1}$ at 5% strain and a similar effect of strain rate on the maximum stress values of the composite was also observed.

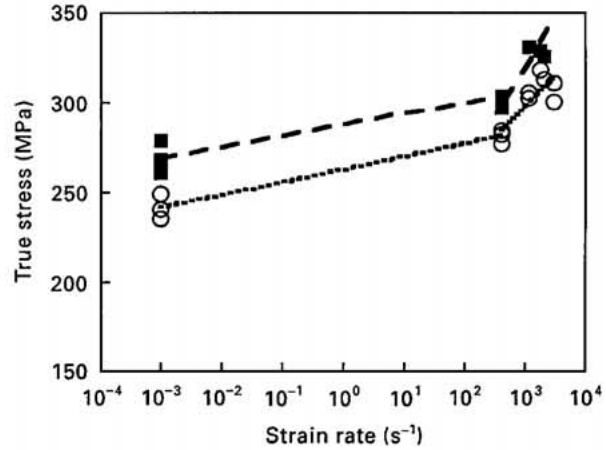

Figure 4 Flow stress (at 5% strain) (·····○·····) and maximum stress (– –■– –) versus strain rate for transverse tests of FP/Al composite.

3.2. Longitudinal direction

Testing of unidirectionally reinforced composites in the longitudinal direction is somewhat problematic in that the deformation and failure modes are strongly dependent upon the precise loading configuration,

and common failure modes include, brooming, kinking and longitudinal splitting. In order to suppress these latter geometrically sensitive failure modes, initial experiments were conducted using several different planar metal end-caps. These caps were simple metal discs, ~2 mm thick and of the same diameter as the bars, placed between the specimen and bar interfaces. The planar end-caps had, in fact, two functions: (a) to prevent premature failure of the composite by brooming, and (b) to protect the faces of the incident and transmitter bars of the SHPB apparatus from being damaged by the stiff fibres.

Brooming was prevented by slight indentation of the composite sample ends into the metal end-caps during testing. Several different types of planar metal end-caps were tried including copper, steel and aluminium. Although the use of this type of end-cap was successful in preventing failure by brooming, it could not give any tractable stress and strain data due to extensive plastic deformation of the end-caps. Because quasi-static testing of the composite in the longitudinal direction showed that the stress–strain curve is non-linear, it was not possible to use the common method of placing strain gauges on the sample and calculating stress values from modulus and measured strain data. The positioning of constraining metal-rings at the specimen ends was also explored but was shown to be unsatisfactory due to sliding of the rings

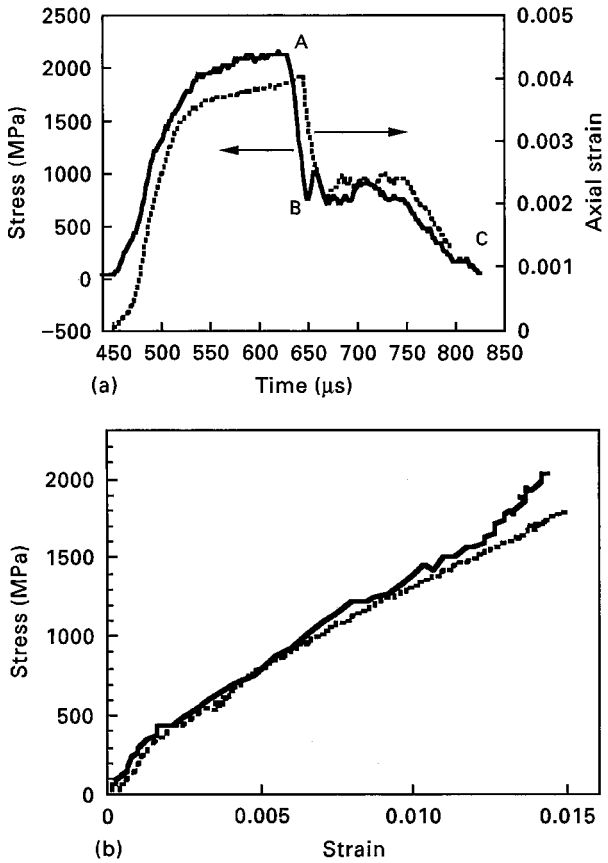

Figure 5 (a) Typical (—) stress and (- - -) axial strain versus time measurement in SHPB compression testing of FP/Al composite in the longitudinal direction. (b) Dynamic and quasi-static stress–strain curves of a composite in the longitudinal direction; strain measured from a strain-gauge mounted on the samples: (—) 400 s^{-1}; (- - -) 10^{-5} s^{-1}.

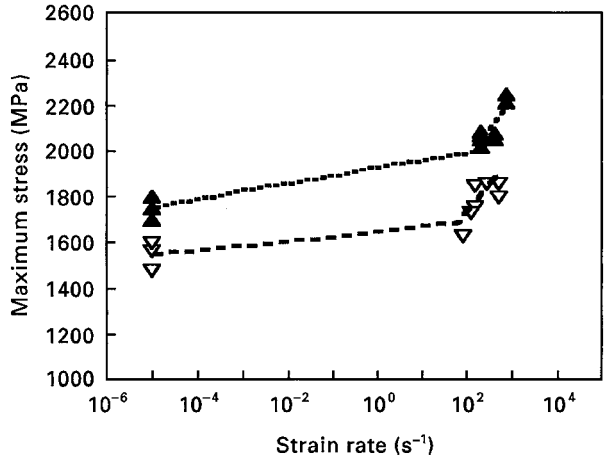

Figure 6 Maximum stress versus strain rate of FP/Al tested using (▽) planar and (▲) recessed tool steel end caps in the longitudinal direction.

on the surface of the specimen during compression testing. Finally, success was achieved through the use of hardened tool steel end-caps with a small recess machined into each. The recess was ~0.5 mm deep and the same diameter as the sample, such that the sample ends were supported and slightly constrained. These recessed end-caps were impedance matched to the SHPB bars.

Fig. 5a presents typical experimental stress and axial strain measurements during high strain-rate testing. In this figure, A represents the maximum stress in the stress curve and is associated with the onset of kinking. After this maximum, the stress quickly decreased until B due to the localization of deformation within the kink region resulting in unloading of the sample between A and B. At point B, deformation started to occur in the kinked region in the form of extensive shearing in the matrix. Finally, at point C, the sample failed completely.

Typical stress–strain curves of the composite up to maximum stress in the longitudinal direction at dynamic and quasi-static strain rates are shown in Fig. 5b. It can be noted that the stress–strain curve is not linear as has been observed previously in the FP/Al composite in the longitudinal direction [4]. The strain corresponding to maximum stress was found to be around 1.5% at both quasi-static and dynamic strain rates. In Fig. 6, the maximum stress is drawn as a function of strain rate for the samples tested using both types of end caps. Use of tool steel inserts promoted early failure in the composite by brooming as depicted in Fig. 6. The stress values increased 300–500 MPa from quasi-static (10^{-5} s^{-1}) to dynamic strain rates (~2×10^2–7×10^2 s^{-1}) on average. This again confirms the strain-rate sensitivity of the maximum stress of the composite within the studied strain-rate range.

4. Microscopy

4.1. Transverse direction

The failure mode in this direction was through shear of the matrix, and the fracture surfaces were inclined,

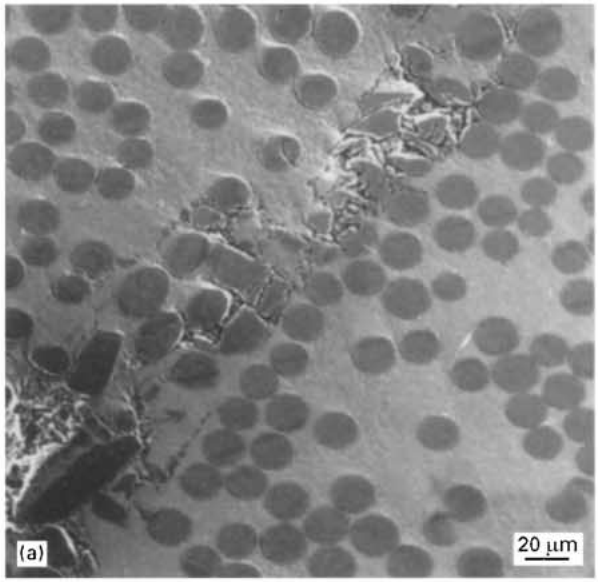

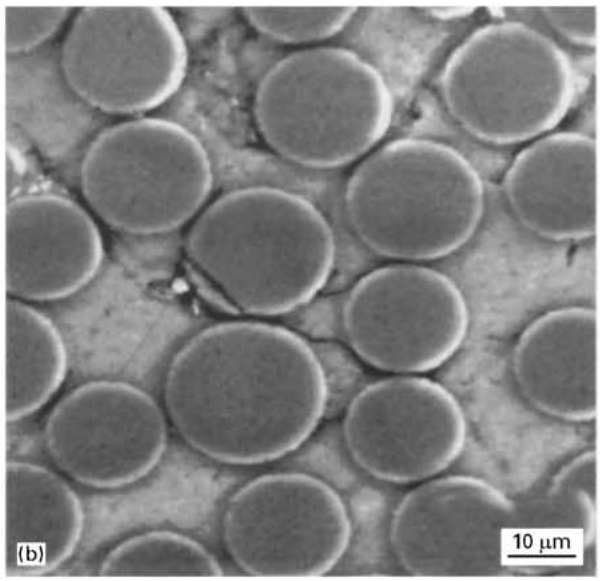

Figure 7 Scanning electron micrographs showing (a) matrix cracking and extensive fibre fracture in a quasi-statically tested specimen, and (b) microcracks between fibres in a dynamically tested specimen.

macroscopically, at 45° to the compression axis. In order to differentiate damage accumulation in the composite at quasi-static and dynamic strain rates, samples tested to approximately the same strain at quasi-strain and dynamic strain rates were cut and metallographically prepared for microscopic observations. The comparison has been performed for samples tested at 10^{-3} and $4 \times 10^{2}\,s^{-1}$ until about 15% strain.

The samples tested quasi-statically showed matrix and extensive fibre fracture in the plane at 45° to the compression axis as shown in Fig. 7a. Close to the matrix crack it is seen that some sections of the circular fibres have become elliptical, showing that fractured and debonded fibres were rotated towards, the fracture plane. This represents a major damage formation mechanism in the composite at this strain rate. In samples tested dynamically, the major damage was microcracks between fibres, Fig. 7b, which might lead to debonding at later stages of deformation. These observations proved that failure in samples tested quasi-statically had initiated earlier, compared to dynamically tested specimens.

4.2. Longitudinal direction

Two types of failure mechanism were observed in this direction: failure resulting from kink formation and failure by brooming. The former mode occurred when recessed end caps were used to support the specimen ends and the latter occurred with planar end caps with which the ends of the samples were not supported. In Fig. 8 typical modes of failure of the composite samples are presented. The first sample of Fig. 8 shows a sample tested using recessed tool steel end caps: the kink formed near to one of the end caps or, rarely, in the middle as previously reported [1, 4]. The second sample of Fig. 8 shows a sample which failed by brooming when a non-indentable planar end cap was used, such as tool steel. The last sample shows kinking of the composite when deformed between relatively soft metal inserts such as Al-6061.

In both failure modes, kinking and brooming, the major damage formation mechanism leading to failure of the composite in compression was buckling of the fibres. However, brooming resulted in lower maximum stresses in the range 1500–1800 MPa for quasi-static and dynamic strain rates, respectively. This is believed to be because of extensive plastic deformation of the matrix resulting from fibre buckling near to one of the unsupported specimen ends. The measured maximum stress may be compared with values reported elsewhere for a similar composite [5]. For example, for $55V_f$% FP fibre composite, the ultimate strength was reported to be around 1500 MPa for an aspect ratio of 1 [5] and 2090 and 2240 MPa when tool steel and mild steel inserts were used to test samples having an aspect ratio of 2 [4]. As noted from the present and previous results, the strength in this direction is greatly dependent on specimen geometry and testing methods.

Typical kink formation in dynamically tested specimens is shown in Fig. 9 and a schematic representation

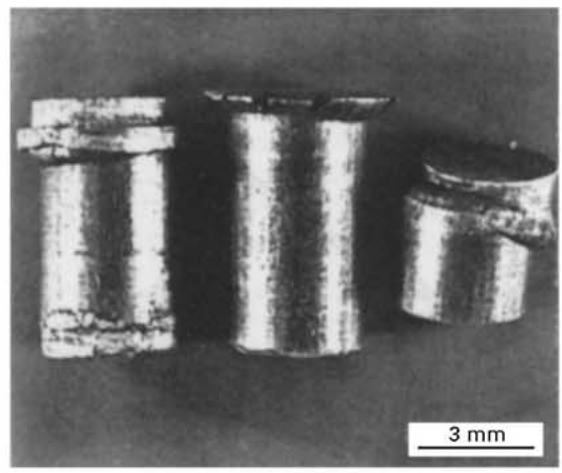

Figure 8 Composite samples tested in longitudinal direction: left, sample tested using recessed tool steel end-caps; centre, sample tested using planar tool steel end-caps; right, sample tested using Al-6061 end-caps.

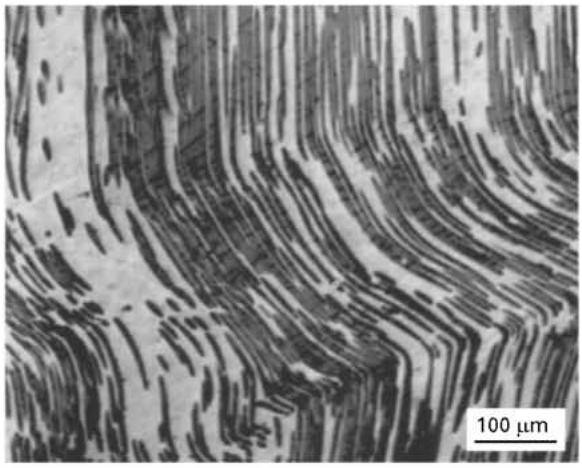

Figure 9 Optical micrograph of kink formation in a dynamically tested specimen.

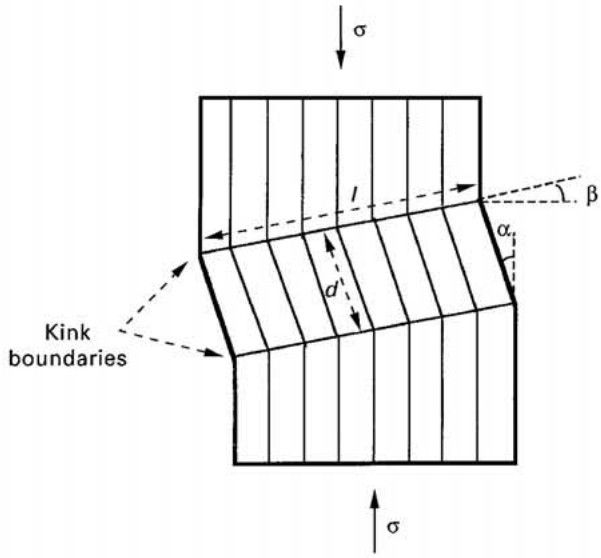

Figure 10 Schematic illustration of kink structure with geometrical parameters.

of kink band formation is illustrated in Fig. 10. The parameters α, β, l and d labelled in Fig. 10 were found to be 40°, 16°, ~ 900 μm and 6.8 mm, respectively. For polymeric composites, typical values of β are given as 20°–30° and α is approximately 2β [6].

Similar geometrical features of kink formation were observed in samples tested quasi-statically. Extensive fibre fracture in the form of buckling was observed at kink boundaries, Fig. 11a, as well as within the kink region, Fig. 11b. It may be noted here that a buckled fibre forms a tensile stress in the matrix on one side of the buckle and a compressive stress at the opposite side. The tensile stresses in the matrix would then tend to form a highly deformed region, Fig. 11b, or voids, Fig. 11a, in the matrix.

The fracture surfaces of these samples confirmed the observations made in Fig. 11. In Fig. 12a, a region of the fracture surface consisting of ductile matrix fracture and buckled fibres is shown. The small fractured but non-separated fibre pieces seen on the top left of fibres in Fig. 12a correspond to the compression side of the buckled fibre. The side opposite these small fibre pieces was under tension and on this side the fibre–matrix interface region had opened up considerably

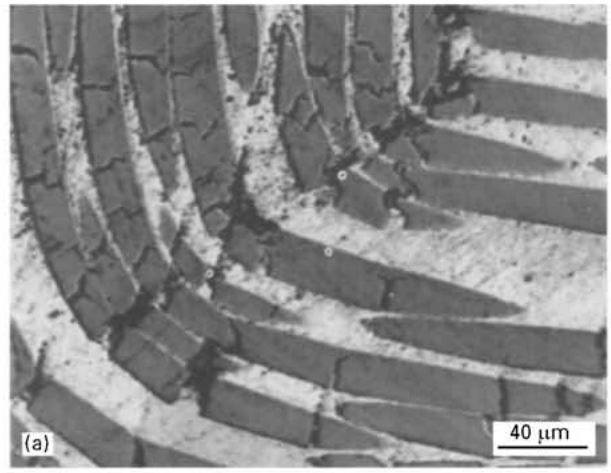

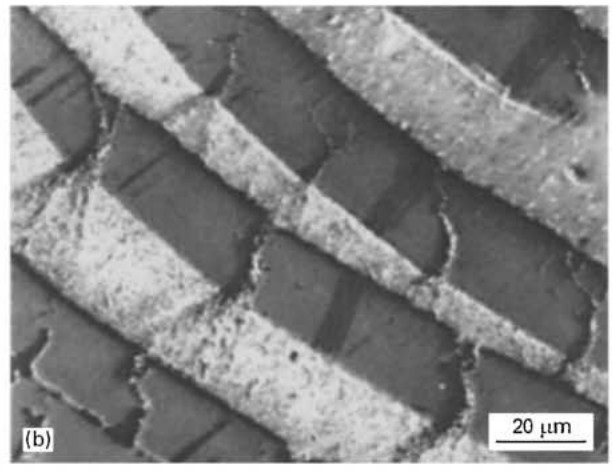

Figure 11 Optical micrographs of fibre fracture (a) at a kink boundary and (b) within the kink region, in dynamically tested specimens.

due to the high local strain. Thus, the fracture shown in Fig. 12a corresponds to a buckled fibre plane at a kink boundary such as that shown in Fig. 11a. Another fracture surface feature is shown in Fig. 12b in which the buckled fibres in the kink region fragmented and then split under the shear strain occurring in the matrix as a result of microbuckling. Note that fibres were split on the same plane corresponding to the kink inclination.

5. Discussion

5.1. Transverse direction

The mechanical properties of unidirectional composites in the transverse direction are dominated by the matrix properties. However, in terms of damage formation the presence of fibres normal to the loading direction in compression is very significant. Typical damage observations made in MMCs include debonding, fibre fracture and crushing and matrix fracture on the maximum shear stress plane at ~45° to the compressive loading axis [7, 8]. High strain-rate testing on C/Al unidirectional composites in the transverse direction has shown that the composite and matrix alloy had similar sensitivity to variation of the strain rate [8]. The observations made in the present study, using considerably larger diameter fibres, are very similar to those given above.

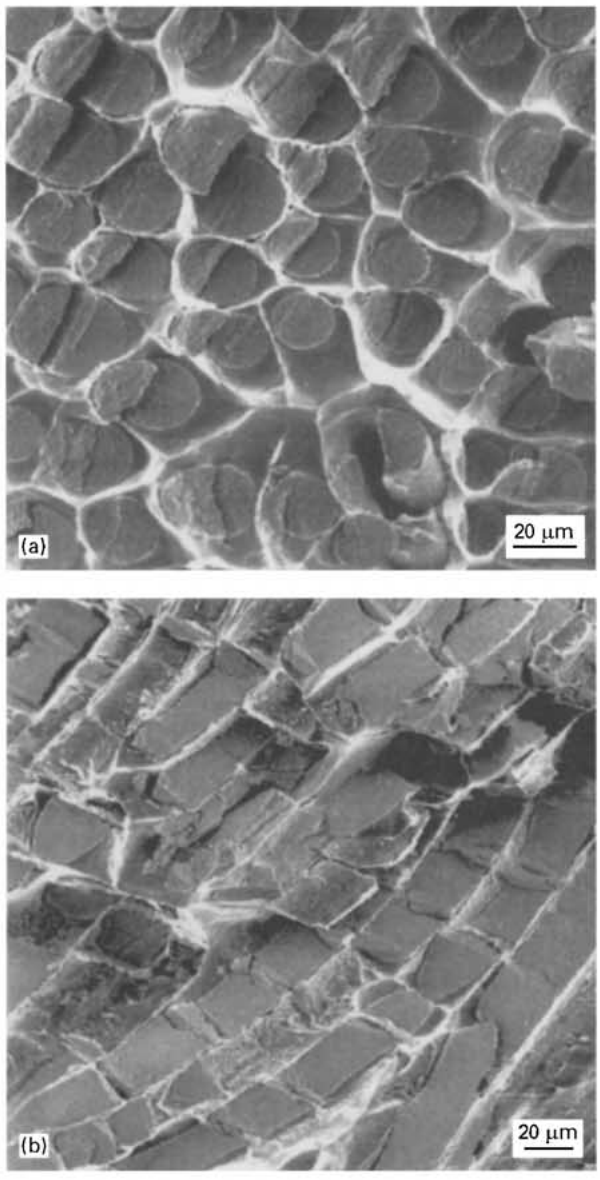

Figure 12 (a) Fracture surface showing compression and tension regions in the dynamically tested specimen. (b) Scanning electron micrograph showing fracture within the kink region in a quasi-statically tested sample.

Therefore, it may also be assumed that the rate-sensitive flow stress behaviour observed in the transverse direction of FP/Al composite is due to strain-rate sensitive flow stress behaviour of the matrix alloy.

The strain-rate dependent flow stress behaviour of metallic materials can be described by several equations depending on the strain-rate regime studied. Until moderate strain rates, $\sim 10^3 s^{-1}$, flow stress is usually expressed as function of the logarithm of strain rate or as a power of the strain rate. The latter was found to fit the present data well (Fig. 4) and is given as

$$\sigma = \sigma_0(\dot{\varepsilon})^n \tag{1}$$

where σ_0 is the flow stress at unit strain rate and n is the strain-rate exponent.

5.2. Longitudinal direction

The failure mechanism at quasi-static and dynamic strain rates was due to plastic microbuckling in the composite. Plastic microbuckling occurs in unidirectional composites consisting of a ductile matrix such as polymeric and metallic matrices.

The existing models of microbuckling are based either on maximum compressive stress corresponding to the onset of the buckling instability followed by kink formation or on the assumption of pre-existing kinks [6]. Applying the former concept, Argon [9] has shown that the critical stress for buckling, σ_{cr}, is

$$\sigma_{cr} = \frac{\tau_y}{\theta} \tag{2}$$

where τ_y is the interlaminar matrix shear strength and θ is the initial fibre misalignment with respect to the compression axis. Argon's equation describes the conditions needed for nucleation of a localized buckling site which then spreads across the specimen at a shear angle. Equation 2 predicts that the onset of the buckling instability is strongly related to matrix yield strength and the initial fibre misalignment. Experimental results on polymeric composites have, in fact, confirmed that σ_{cr} is directly proportional to the matrix yield strength and that θ is around 3° [10]. Jelf and Fleck have further applied Argon's equation to several different model composites resembling MMCs and found excellent agreement between experimental and measured values [10].

The morphology of kink formation has been summarized by Evans and Adler [11] and is reproduced schematically in Fig. 13. If the fibres are well-bonded, as they are in the composite studied here, the matrix within the kink must be subjected to a shear strain, ϕ, as shown in Fig. 13. Therefore, the regions A′B′C and AOB must be experiencing a large localized strain which may lead to void formation. The actual microstructural analogue of Fig. 13 is shown in Fig. 11a and b and the localized region of plastic deformation is very clearly seen, particularly in Fig. 11b.

Using the above analysis and knowledge, the mechanical response of the present composite might be clarified to some extent. For example, Equation 2 can be applied in order to estimate matrix shear strength by using the experimentally determined failure strength and an initial fibre misorientation of 4°. By taking the critical buckling stress as the quasi-static maximum stress ($\sim$1750 MPa), the matrix shear stress was found to be $\sim$125 MPa, a value which might be reasonably expected for the matrix alloy studied.

The observed strain-rate dependent maximum stress of the composite in the longitudinal direction can be understood by considering the stress amplification which occurs during kink accommodation. Lankford [12] showed the strength of the composite, σ_c, experiencing kinking is

$$\sigma_c = \sigma_0 + \left(\frac{El}{C_s}\right)\dot{\varepsilon} \tag{3}$$

where σ_0 and E are the quasi-static composite compressive strength and modulus, l is the kink propagation length, C_s is the shear velocity. The second term in Equation 3 is due to the stress magnification by kink propagation and is plotted separately in Fig. 14. For

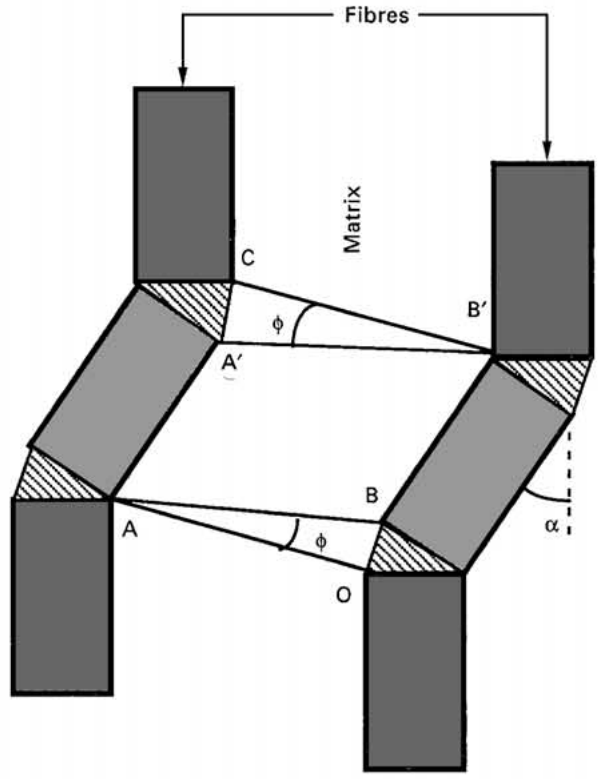

Figure 13 Morphology of kink formation in a composite with a strong interface.

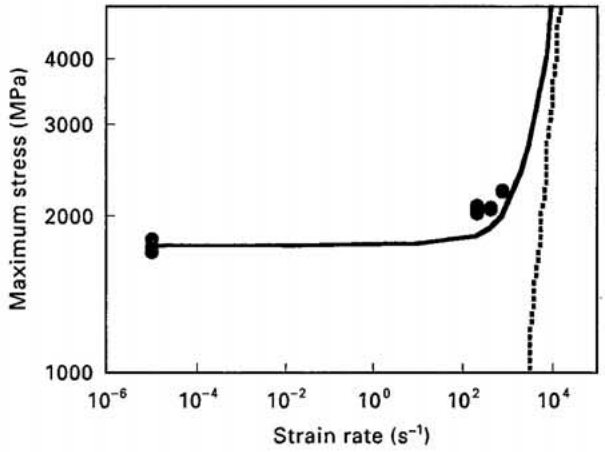

Figure 14 Comparison of maximum stress data obtained (●) experimentally and (——) using Equation 3. (- - -) Kink propagation.

the purpose of testing the applicability of the Equation 3 to the present composite maximum stress data, the following values of the various parameters are used in Equation 3: $\sigma_0 \sim 1750\,\text{MPa}$, $E \simeq 150\,\text{GPa}$, $l \simeq 7\,\text{mm}$ and $C_s \simeq 3200\,\text{m s}^{-1}$. In Fig. 14 results of calculations together with experimental maximum stress data are shown. According to Equation 3 and present calculations shown in Fig. 14, the kink propagation term becomes increasingly important when the strain rate exceeds $\sim 10^2\,\text{s}^{-1}$. The experimental stress values shown in Fig. 14 matched the calculated stress values quite satisfactorily: adjustment of the parameters in Equation 3, or possibly more accurately measured values of these parameters, could improve agreement even more. In any event, the trends in experimental and calculated stress values are almost identical.

It should also be mentioned that the strain rates considered here are macroscopic and are calculated using measured strain values. However, the strain rates in the kink region would locally reach very high values as noted previously [12]. For example, the measured strain value corresponding to maximum stress for the present FP/Al was about 0.015, while the local strains measured from Fig. 11b and shown as ϕ in Fig. 13 are about 1.5 just after kink formation. This corresponds, therefore, to a local strain rate which is of the order of 100 times higher than the macroscopic strain rate: consequently, the contribution of this part of the deformation to the overall strengthening effect is greatly increased.

6. Conclusion

The mechanical response of an FP/Al composite has been determined in the transverse and longitudinal directions in compression. It is found that the composite in the transverse direction exhibited strain-rate sensitivity of the flow stress (at 5% strain) and maximum stress within the studied strain rate range (10^{-3}–$3 \times 10^{-3}\,\text{s}^{-1}$). Damage formation in this direction was observed microscopically to be initiated at relatively low stresses and strains at quasi-static rates as compared to high strain rates. In the longitudinal direction, the composite maximum stress was found to be strain-rate sensitive. The observed rate-sensitive flow and maximum stresses of the composite are well described in terms of strain-rate dependent kink-band propagation.

Acknowledgements

The authors gratefully acknowledge financial support from the Army Research Office, award DAAH04-95-2-0001. One of the authors (MG) also gratefully acknowledges financial support from the Izmir Institute of Technology, Turkey.

References

1. A. R. CHAMPION, W. H. KRUEGER, H. S. HARTMAN and A. K. DHINGRA, in "Proceedings of the 2nd International Conference on Composite Materials", Toronto, Canada (1978) p. 883.
2. M. GUDEN and I. W. HALL, *Mater. Sci. Eng.* **A232** (1997) 1.
3. P. S. FOLLANSBEE, "Metals Handbook", vol. 8 (ASM, Metals Park, OH, 1985) pp. 198–203.
4. H. R. SHETTY and T.-W. CHOU, *Metall. Trans.* **16A** (1985) 853.
5. J. C. HUANG and Y.-S. LO, *Mater. Chem. Phys.* **35** (1993) 71.
6. J. LANKFORD, *J. Mater. Sci.* **30** (1995) 4343.
7. B. J. WENG, S. T. CHANG and S. E. HSU, *Mater. Sci. Eng.* **A156** (1992) 143.
8. C. C. POTEET and I. W. HALL, *ibid.* **A222** (1997) p. 35.
9. A. S. ARGON, in "Treatise on Materials Science and Technology", vol. 1 (Academic Press, New York, 1972) p. 79.
10. P. M. JELF and N. A. FLECK, *J. Compos. Mater.* **26** (1992) 2706.
11. A. G. EVANS and W. F. ADLER, *Acta Metall.* **26** (1978) 725.
12. J. LANKFORD, *Mater. Sci. Eng.* **A107** (1989) 261.

Received 28 May 1997
and accepted 2 April 1998